Accurate elastic scattering cross sections for 17-MeV deuterons*

J. D. Childs, W. W. Daehnick, and M. J. Spisak
Nuclear Physics Laboratory, University of Pittsburgh, Pittsburgh, Pennsylvania 15260
(Received 14 December 1973)

Angular distributions for 17.0-MeV (d,d) scattering on 23 isotopically pure targets (^{27}Al, ^{48}Ca, ^{51}V, ^{52}Cr, ^{54}Fe, ^{56}Fe, ^{59}Co, ^{58}Ni, ^{62}Ni, ^{64}Ni, ^{68}Zn, ^{89}Y, ^{93}Nb, ^{100}Mo, ^{105}Pd, ^{112}Cd, ^{115}In, ^{112}Sn, ^{120}Sn ^{124}Sn, ^{208}Pb, ^{209}Bi, ^{232}Th) have been measured from $\theta_{lab} \leq 10$ to 165° in 5° steps. Relative experimental errors are always less than 2% and absolute scale errors range from 2 to 5%. Optical model searches have been performed on all angular distributions. Good fits were obtained (with four free parameters) for three values of the real radius parameter $r_0 = 1.0$, 1.1, and 1.2 fm using starting values of $V_0 \approx 100$ MeV. The best fit parameters are presented for these searches, as well as for the best over-all nine-parameter fits. The data show some preference for parameter values close to $r_0 = 1.1$ fm (with $a \approx 0.82$) for all targets heavier than ^{48}Ca, although very acceptable fits are also obtained for all three sets with restricted parameters. The searches with nine free parameters resulted in overly perfect fits ($\chi^2 \lesssim 1$) indicative of considerable ambiguity for so large a parameter space. Preliminary global fits to our 17-MeV data yielded a formula for generating usable optical model parameters for other near-spherical nuclei of mass $A > 48$.

NUCLEAR REACTIONS ^{27}Al, ^{48}Ca, ^{51}V, ^{52}Cr, ^{54}Fe, ^{56}Fe, ^{59}Co, ^{58}Ni, ^{62}Ni, ^{64}Ni, ^{68}Zn, ^{89}Y, ^{93}Nb, ^{100}Mo, ^{105}Pd, ^{112}Cd, ^{115}In, ^{112}Sn, ^{120}Sn, ^{124}Sn, ^{208}Pb, ^{209}Bi(d,d), $E = 17.00$ MeV, measured $\sigma(\theta)$ and ^{232}Th(d,d'), $E = 17.00$ MeV, measured $\sigma(E_d,\theta)$ optical model analysis, deduced A dependence in optical model parameter prescription. Enriched targets.

I. INTRODUCTION

Deuteron-induced reactions have been most valuable in nuclear structure studies and, consequently, a fairly large number of deuteron scattering experiments has been reported in recent years.[1-14] In most of these studies a limited number of isotopes were investigated at one particular energy in the region from 11.8 to 52 MeV. Concurrent or subsequent optical model[15] analyses have been very successful in fitting subsets of the known data with reasonable parameters.[16-21]

The present study was undertaken as a starting point for a "global," i.e., simultaneous, optical model analysis of several comprehensive data sets for a variety of targets and energies. Such a study requires accurately normalized data so that a target-to-target comparison will truly reflect nuclear effects and not experimental scale uncertainties.

Experimentally, the present work fills a data gap at 17 MeV, an energy region very important to current Van de Graaff accelerators, and also aims at noticeably improved accuracy (≈ 2%) in order to reduce optical model parameter ambiguities caused by large error bars. Particular care was taken to reduce systematic (scale) errors which strongly affect optical model parameters deduced from the relatively structureless angular distributions for heavy isotopes.[22] The starting parameters for optical model searches were guided by potentials and volume integrals suggested by folding calculations.[23-30] The geometrical parameters were kept in a range consistent with scattering results at higher energies. At the same time spin-orbit parameters were fixed by recently published polarization data.[31]

Portions of this work and a preliminary global analysis (for 17-MeV data only) have been presented previously.[32,33] A future paper will report global analyses which include data for several other energies as well as those for 17 MeV.

II. EXPERIMENTAL CONSIDERATIONS

A. General

The elastic scattering measurements were designed to keep individual contributions from all controllable experimental errors below 1%. One procedure used was to take the same data points under different experimental conditions. Points would be remeasured using different solid angles, detectors, amplifiers, beam currents, analog-to-digital computers, targets (if possible), etc. The electronic setup was kept simple so as not to introduce additional sources of error.

Our random errors (given below) reflect the reproducibility in the shape of angular distributions from day to day. The absolute or scale error derives from both the *absolute* reproducibility of data points taken under different conditions, and also additional factors such as target thickness

uncertainty, solid angle determination, etc.

The major contribution to absolute errors turned out to be the uncertainty in the determination of target thicknesses.

B. Experimental procedure

Measurements were performed in our new 66 cm (aluminum) scattering chamber which has a number of special features (see Fig. 1). The target ladder and turntable axis are located 7.6 cm upstream from the geometric center of the chamber in order to permit the longer target-to-detector distances at low scattering angles (33 cm for $\theta \leq \pm 60°$) of a larger chamber without the accompanying increased chamber volume and expense. A 1200 liter/sec oil diffusion pump with freon baffle easily reaches and maintains a pressure of $\sim 10^{-6}$ Torr. The turntable is cooled to $\lesssim -30°C$ with freon lines which are also fed through a stationary (monitor) detector platform at the rear of the chamber. Thus, cooled surface barrier detectors may be used both for data taking and as monitors. Cooled detectors can be operated at lower noise for increased bias voltages, which cause a significant reduction in the tails of peaks.[34] Behind the chamber is mounted a deep Faraday cup whose entrance aperture subtends a cone of $\pm 3.75°$ opening with respect to the target. This entrance slit shields the electron suppressor ring and the edge of the Faraday cup from any beam scattered by the target. The suppressor was maintained at a potential of -285 V. Defining slits for the entering beam can be placed at various positions in an insulated slit holder located inside the chamber (see Fig. 1). An insulated antiscattering slit is also provided with separate current metering. Further collimation can be done with one or both of the two beam line slits, located outside the chamber, 50.8 cm and 30.5 cm from the target. Beam divergence is controlled with a slit located upstream just after the quadrupole focusing lens.

A counter array of four fully depleted 100 mm^2 surface barrier detectors, 1000 μm thick, was mounted at the positions θ, $\theta+10°$, $\theta+20°$, $\theta+30°$ on the turntable, while two monitor detectors were placed symmetrically about the beam axis at ± 20 or $\pm 30°$. All detectors were equipped with electron deflector magnets. (Initially, data were taken with counter telescopes; however, it was found eventually that more data as well as more accurate cross sections were obtained with a set of specially selected single counters with absorbers.)

The electronic setup is indicated in Fig. 2. Two independent multichannel analyzers received signals from the six detectors. Actually, eight spectra are registered, as the outputs of two detectors are fed to both analyzers for electronic uniformity and reliability checks. Monitor detector outputs were also fed into scalers and employed as clock pulses for the analyzer with uncorrelated spectra to obtain dead time corrections.

Measurements were made in 5° steps from $\theta_{lab} \leq 10$ to 165°. The lowest angle cross sections are most sensitive to scattering angle θ errors.

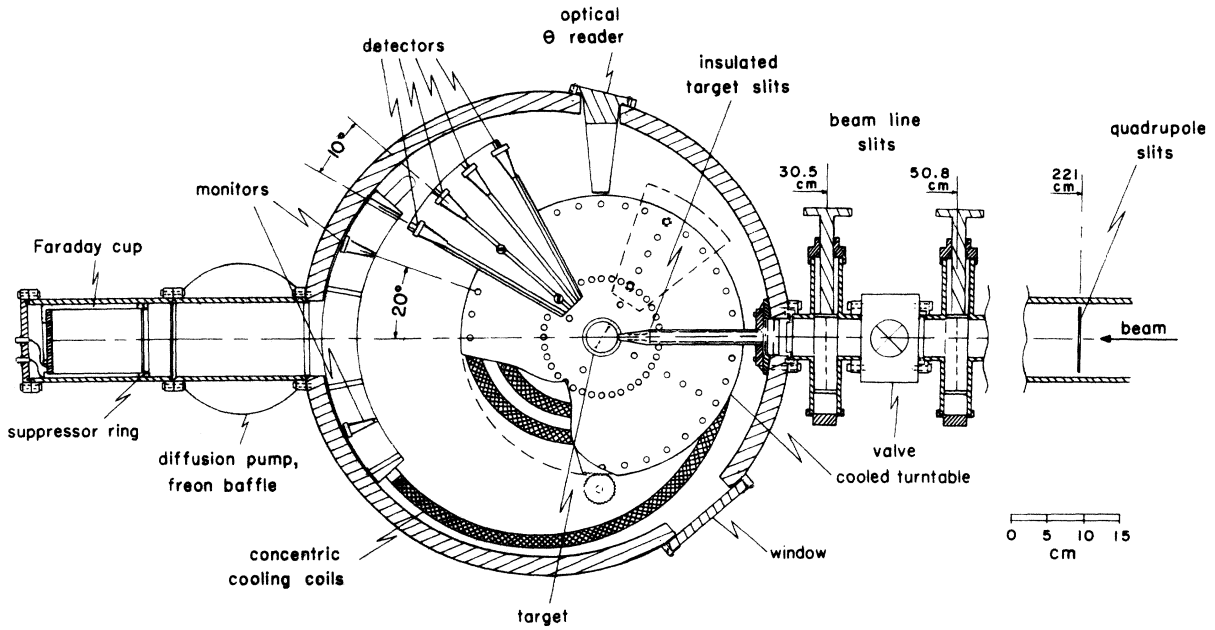

FIG. 1. Schematic diagram of (Pittsburgh) 66 cm scattering chamber. Slit distances measured with respect to target.

Hence for very small angle runs systematic errors were minimized by measuring $\sigma(\theta)$ on both sides of the ($\theta = 0$) beam axis. The $\theta_{lab} = 5°$ points were taken for seven of the targets by measuring relative yields at ± 5 and $\pm 15°$ simultaneously, correcting for scattering angle shift, and then normalizing to the 15° points for which absolute cross sections were found.

Particle discrimination between deuteron-induced reaction products is a necessity since most (d, p) and (d, α) reactions have positive Q values. The technique employed was to use 1.0 mm thick, fully depleted detectors, along with carefully varied aluminum absorbers to degrade the α spectrum sufficiently below the deuteron elastic peak. 1 mm detectors just stop 17-MeV deuterons, and yet will only stop protons with a maximum energy of 12 MeV. A typical spectrum is shown in Fig. 3. Although the deuteron resolution is worsened due to straggling in the absorber, the elastic peak stands out clearly from the other reaction products. The typical peak-to-background ratio obtained was $\gtrsim 500{:}1$.

A set of "standard" natural platinum targets cut from one piece of rolled ~2.5 μm thick Pt foil was used for run-to-run normalization checks. Platinum was chosen because of its high charge number, chemical stability, and foil uniformity.

Periodically, the standard platinum target was bombarded with a proton beam of $E \approx 8$ MeV, for which pure Rutherford scattering could be assumed for low angles. Then, without disturbing the defining detector apertures, Al absorbers were inserted between apertures and detectors, and the targets exposed to 17-MeV deuterons.

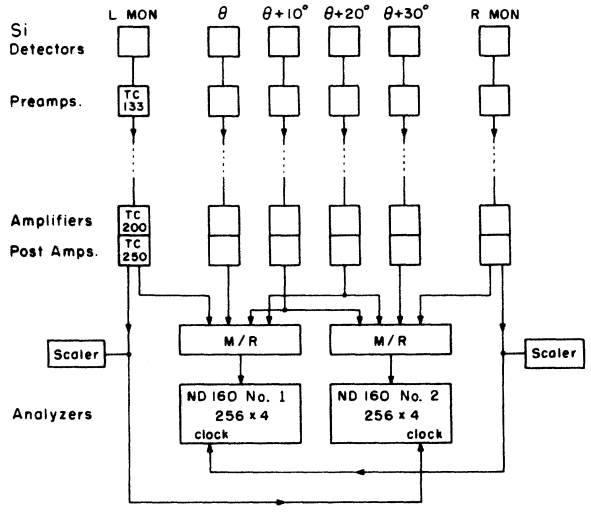

FIG. 2. Electronics block diagram.

Given the known Pt foil thickness, the proton scattering determined the effective solid angles of the detectors.

At the beginning and end of each series of runs, the Pt target was put in the deuteron beam, and measurements were repeated at several standard scattering angles. Thus the solid angles and "efficiencies" of the detector configuration being used that day were verified or determined from the already known $Pt(d, d)$ cross sections. Moreover, any shift in the scattering angle (θ) calibration could be noted and corrected for to within 0.1° by adjusting the scattering angle reader prior to other data taking.

During the measurements for an angular distribution the target angle α with respect to the beam usually has to be changed. The fixed monitors were used to determine an effective target thickness by renormalizing all data via the monitor yields relative to runs with $\alpha = 0°$ target angle. The ratio of the counter monitor yield to the integrated charge remained constant to within 1% for run series with a fixed target angle α.

C. Target thickness determination

Whenever possible, target thicknesses were determined by weighing and measuring the self-supporting foils before mounting. This procedure was used with ^{27}Al, ^{52}Cr, ^{56}Fe, Pt, and ^{232}Th.

All foils were also measured for thickness with low energy proton and α beams. Measurements were first made at $\pm 25°$ to correct for any zero degree shift. A subsequent measurement with all four detectors of the array could then be compared to pure Rutherford scattering at the measured angles of 25, 35, 45, and 55°. Each target was measured at least twice in this fashion, with one or more factors different: usually bombarding

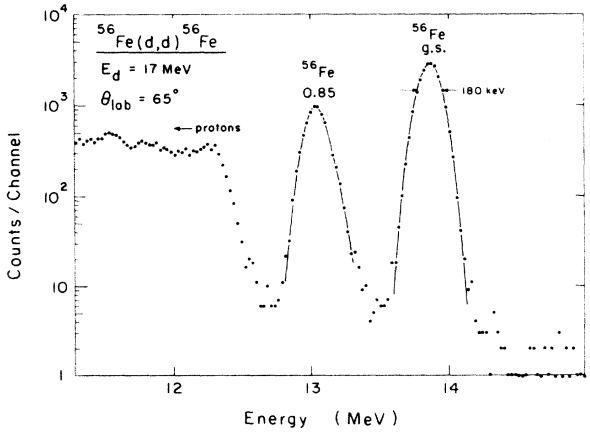

FIG. 3. Representative semilog plot of 17-MeV (d, d) data taken with 1 mm detector plus 0.25 mm Al absorber. Note sharp cutoff of proton counts near 12.5 MeV.

particle type or incident energy. Corrections were computed for energy loss in the target, outscattering from the Faraday cup, and finite solid angle of the detectors.

Checks for macroscopic target nonuniformities were made by moving the target vertically in the beam between runs. After the beam was focused it approximately filled the target defining slit of 1×3 mm^2, and three runs were taken: with the target centered, with the target raised 3 mm, and with the target lowered by the same amount.

D. Target composition

Table I is a list of all targets used, including isotopic purity, thickness, and uniformity. All were self-supporting foils except for ^{208}Pb and ^{209}Bi, which, because of their low melting points, had been evaporated onto 0.24 mg/cm^2 Al backings for better beam heat dissipation.

The ^{27}Al elastic peak interfered with the ^{208}Pb and ^{209}Bi peaks at $\theta_{lab} \leq 30°$, but since an angular distribution of ^{27}Al was also measured separately, the "impurity" contribution from the backing material could be readily subtracted. The only other target with a significant contamination was the ^{58}Ni foil, which had a cracked carbon layer on it. The carbon peak began to interfere with the elastic Ni peak at $\theta_{lab} \leq 20°$. But as it amounted to only a few per cent of the nickel yield, it was deemed sufficient to subtract out the ^{12}C counts predicted from an average carbon optical model angular distribution[20] matched to the well-separated peaks at $\theta_{lab} > 20°$.

TABLE I. Target data.

Target	Thickness (mg/cm^2)	Uniformity (%)	Isotopic purity (%)
^{27}Al	7.75 ±1%	1	(100)
^{48}Ca	1.0 ±5%	?	96[a]
^{51}V	0.726±2%	3	(100)
^{52}Cr	0.684±1%	1	99.9
^{54}Fe	0.384±2%	1	98[a]
^{56}Fe	0.924±2%	1	99.9
^{59}Co	0.774±1%	1	(100)
^{58}Ni	0.372±3%	1	99
^{62}Ni	4.80 ±2%	2	98
^{64}Ni	1.02 ±3%	2	95
^{68}Zn	0.750±1%	5	99
^{89}Y	1.024±1%	1	(100)
^{93}Nb	0.810±1%	1	(100)
^{100}Mo	1.06 ±1.5%	3	90
^{105}Pd	1.87 ±1%	1	98[a]
^{112}Cd	2.14 ±1.5%	2	98[a]
^{115}In	2.60 ±1.5%	2	99
^{112}Sn	2.56 ±1%	1.5	75
^{120}Sn	2.45 ±3.5%	2	96
^{124}Sn	1.21 ±3.5%	9	96
^{nat}Pt	5.85 ±1%	1	...
^{208}Pb	0.690±1%	1	99.1
^{209}Bi	0.139±1%	1.5	(100)
^{232}Th	1.03 ±2%	3	(100)

[a] Estimated.

E. Contributions from low-lying excited states

To examine deuteron spectra for possible inelastic states unresolved from the ground state we employed magnetic analysis and a position sensitive detector in the focal plane of our Enge split-pole spectrograph. Particle and position identification was accomplished with our on-line PDP-15/40 computer and use of the data analysis code CRUNCH.[35] The only competing reaction products, tritons, were found to have negligible cross sections for the cases investigated. Significant corrections for inelastic scattering were needed only for ^{232}Th.

The known 30-keV state in ^{93}Nb was searched for in the spectrograph at 40, 90, and 140° and was found to be insignificant compared to the elastic peak at all three angles. However, the first 2^+ and 4^+ states of ^{232}Th (at 50 and 162 keV, respectively) are strongly excited relative to the ground state at high angles. Therefore, ^{232}Th-(d, d') spectra were taken in the spectrograph from $\theta_{lab} = 45$ to 140° in 5° steps with a resolution of ~20 keV (see Fig. 4). The experiment was repeated in the standard scattering chamber in order to obtain better absolute cross sections. Here the elastic group with a resolution of 150 keV (straggling) encompassed the first three states. The angular distribution of the ground state was extracted by using the relative peak ratios known from the spectrograph runs.

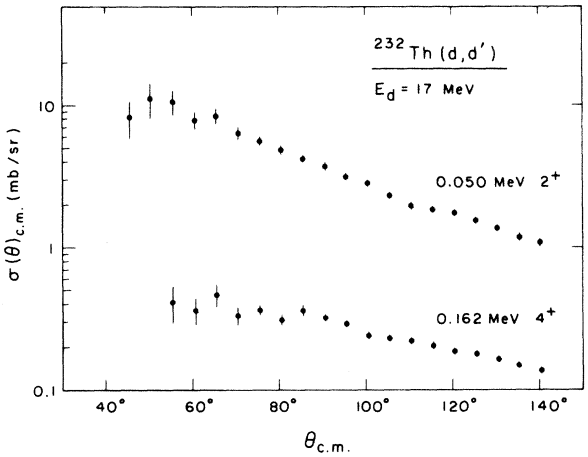

FIG. 4. Angular distributions for the first two excited states of ^{232}Th obtained from inelastic deuteron scattering.

TABLE II. 17-MeV elastic deuteron scattering data: Σ_{abs} is absolute error, Σ_{rel} is relative error, c.m. angle (app) is approximate center of mass angle. The notation E ± n means "$\times 10^{\pm n}$."

^{27}Al(d,d) Σ_{abs} = 2.0% Σ_{rel} = 2.0%		^{48}Ca(d,d) Σ_{abs} = 5.0% Σ_{rel} = 5.0%		^{51}V(d,d) Σ_{abs} = 4.0% Σ_{rel} = 2.0%		^{52}Cr(d,d) Σ_{abs} = 2.0% Σ_{rel} = 2.0%		^{54}Fe(d,d) Σ_{abs} = 2.0% Σ_{rel} = 2.0%		^{56}Fe(d,d) Σ_{abs} = 3.0% Σ_{rel} = 2.0%	
c.m. angle (deg)	$\sigma_{c.m.}$ (mb/sr)	c.m. angle (deg)	$\sigma_{c.m.}$ (mb/sr)	c.m. angle (deg)	$\sigma_{c.m.}$ (mb/sr)	c.m. angle (deg)	$\sigma_{c.m.}$ (mb/sr)	c.m. angle (deg)	$\sigma_{c.m.}$ (mb/sr)	c.m. angle (deg)	$\sigma_{c.m.}$ (mb/sr)
10.7	7.61 E + 3	20.5	1.45 E + 3	5.2	6.04 E + 5	10.4	2.89 E + 4	10.4	3.80 E + 4	5.2	7.60 E + 5
16.1	2.21 E + 3	25.7	3.18 E + 2	10.4	2.85 E + 4	15.6	6.36 E + 3	15.6	7.80 E + 3	10.4	3.63 E + 4
21.5	6.35 E + 2	30.9	1.44 E + 2	15.6	6.21 E + 3	20.8	1.57 E + 3	20.7	2.01 E + 3	15.5	7.58 E + 3
26.8	1.18 E + 2	41.2	5.47 E + 1	20.8	1.58 E + 3	25.9	3.28 E + 2	25.9	4.32 E + 2	20.7	1.84 E + 3
32.1	4.16 E + 1	46.4	2.53 E + 1	26.0	3.07 E + 2	31.1	1.38 E + 2	31.1	1.83 E + 2	25.9	4.11 E + 2
34.8	5.24 E + 1	51.5	2.49 E + 1	31.1	1.28 E + 2	36.3	1.22 E + 2	36.2	1.46 E + 2	31.0	1.96 E + 2
37.4	6.15 E + 1	56.7	2.98 E + 1	36.8	1.16 E + 2	41.4	7.60 E + 1	41.4	9.30 E + 1	36.2	1.55 E + 2
40.1	6.14 E + 1	61.8	2.29 E + 1	41.5	7.46 E + 1	46.6	3.71 E + 1	46.5	4.55 E + 1	41.3	8.92 E + 1
42.8	5.22 E + 1	66.9	1.30 E + 1	46.6	3.61 E + 1	51.7	2.14 E + 1	51.6	2.43 E + 1	46.5	3.93 E + 1
45.4	3.87 E + 1	72.0	4.82 E + 0	51.7	2.10 E + 1	56.8	1.57 E + 1	56.8	1.61 E + 1	51.6	2.10 E + 1
48.0	2.50 E + 1	77.0	2.02 E + 0	56.9	1.55 E + 1	61.9	8.83 E + 0	61.8	9.49 E + 0	56.7	1.47 E + 1
50.6	1.32 E + 1	82.1	3.51 E + 0	62.0	8.36 E + 0	67.0	3.36 E + 0	66.9	4.45 E + 0	61.8	8.77 E + 0
53.3	5.49 E + 0	87.1	5.46 E + 0	67.0	2.90 E + 0	72.1	2.06 E + 0	72.0	3.06 E + 0	66.9	4.25 E + 0
55.9	2.12 E + 0	92.1	5.10 E + 0	72.1	1.92 E + 0	77.2	3.36 E + 0	77.1	4.00 E + 0	71.9	3.32 E + 0
58.5	1.69 E + 0	97.1	4.05 E + 0	77.2	3.66 E + 0	82.2	4.30 E + 0	82.1	4.44 E + 0	77.0	3.90 E + 0
61.1	2.94 E + 0	102.1	2.26 E + 0	82.2	4.78 E + 0	87.2	3.50 E + 0	87.1	3.92 E + 0	82.0	3.89 E + 0
63.7	4.59 E + 0	107.0	1.38 E + 0	87.3	3.91 E + 0	92.2	1.86 E + 0	92.1	1.69 E + 0	87.1	2.60 E + 0
66.3	5.84 E + 0	112.0	1.02 E + 0	92.3	2.08 E + 0	97.2	6.23 E − 1	97.1	5.72 E − 1	92.1	1.05 E + 0
68.9	6.40 E + 0	116.9	9.79 E − 1	97.3	7.00 E − 1	102.2	2.64 E − 1	102.1	3.62 E − 1	97.1	3.59 E − 1
71.4	6.34 E + 0	121.8	7.46 E − 1	102.2	3.29 E − 1	107.2	5.07 E − 1	107.1	6.99 E − 1	102.0	4.17 E − 1
74.0	5.34 E + 0	126.7	1.44 E + 0	107.2	6.39 E − 1	112.1	8.36 E − 1	112.0	1.00 E + 0	107.0	7.16 E − 1
76.6	4.39 E + 0	131.6	1.51 E + 0	112.1	1.02 E + 0	117.0	8.96 E − 1	116.9	9.98 E − 1	111.9	8.52 E − 1
79.1	3.26 E + 0	141.3	1.25 E + 0	117.0	1.14 E + 0	121.9	7.20 E − 1	121.8	7.28 E − 1	116.9	7.24 E − 1
84.2	1.58 E + 0	150.9	8.76 E − 1	122.0	9.29 E − 1	126.8	4.49 E − 1	126.8	4.08 E − 1	121.8	4.50 E − 1
89.3	8.31 E − 1			126.9	5.92 E − 1	131.7	2.38 E − 1	131.6	2.00 E − 1	126.7	2.19 E − 1
94.3	6.55 E − 1			131.7	3.32 E − 1	136.6	1.44 E − 1	136.5	1.56 E − 1	131.6	1.22 E − 1
99.3	6.61 E − 1			136.6	2.06 E − 1	141.4	1.40 E − 1	141.4	2.13 E − 1	136.5	1.34 E − 1
104.2	7.02 E − 1			141.5	1.89 E − 1	146.3	1.71 E − 1	146.2	2.92 E − 1	141.3	1.89 E − 1
				146.3	2.25 E − 1	151.1	2.14 E − 1	151.1	3.47 E − 1	146.2	2.29 E − 1
				151.1	2.88 E − 1	155.9	2.46 E − 1	155.9	3.44 E − 1	151.0	2.33 E − 1
				156.0	3.66 E − 1	160.8	2.62 E − 1	160.7	2.92 E − 1	155.9	2.02 E − 1
				160.8	4.27 E − 1	165.6	2.47 E − 1	165.6	2.17 E − 1	160.7	1.68 E − 1
				165.6	4.19 E − 1					165.5	1.16 E − 1

TABLE II *(Continued)*

^{89}Y c.m. angles used.

Lab angle (exact)	c.m. angle (app.)	^{58}Ni(d,d) $\Sigma_{abs}=3.0\%$ $\Sigma_{rel}=2.0\%$ $\sigma_{c.m.}$ (mb/sr)	^{59}Co(d,d) $\Sigma_{abs}=2.0\%$ $\Sigma_{rel}=2.0\%$ $\sigma_{c.m.}$ (mb/sr)	^{62}Ni(d,d) $\Sigma_{abs}=5.0\%$ $\Sigma_{rel}=2.0\%$ $\sigma_{c.m.}$ (mb/sr)	^{64}Ni(d,d) $\Sigma_{abs}=3.0\%$ $\Sigma_{rel}=2.0\%$ $\sigma_{c.m.}$ (mb/sr)	^{68}Zn(d,d) $\Sigma_{abs}=4.0\%$ $\Sigma_{rel}=2.0\%$ $\sigma_{c.m.}$ (mb/sr)	^{89}Y(d,d) $\Sigma_{abs}=2.0\%$ $\Sigma_{rel}=2.0\%$ $\sigma_{c.m.}$ (mb/sr)	^{93}Nb(d,d) $\Sigma_{abs}=3.0\%$ $\Sigma_{rel}=2.0\%$ $\sigma_{c.m.}$ (mb/sr)	^{100}Mo(d,d) $\Sigma_{abs}=4.0\%$ $\Sigma_{rel}=2.0\%$ $\sigma_{c.m.}$ (mb/sr)	^{105}Pd(d,d) $\Sigma_{abs}=2.0\%$ $\Sigma_{rel}=2.0\%$ $\sigma_{c.m.}$ (mb/sr)
5.0	5.1	...	8.31 E +5	9.34 E +5	...	...	1.94 E +6	2.10 E +6	...	...
10.0	10.2	4.80 E +4	4.27 E +4	4.29 E +4	4.52 E +4	5.56 E +4	1.12 E +5	1.23 E +5	1.33 E +5	1.55 E +5
15.0	15.3	9.56 E +3	8.12 E +3	8.15 E +3	8.57 E +3	1.07 E +4	1.94 E +4	2.18 E +4	2.39 E +4	2.90 E +4
20.0	20.4	2.37 E +3	1.97 E +3	1.89 E +3	1.98 E +3	2.52 E +3	4.99 E +3	5.60 E +3	5.99 E +3	7.82 E +3
25.0	25.6	5.34 E +2	4.36 E +2	4.51 E +2	4.76 E +2	6.45 E +2	1.55 E +3	1.74 E +3	1.79 E +3	2.40 E +3
30.0	30.6	2.56 E +2	2.35 E +2	2.57 E +2	2.96 E +2	3.76 E +2	6.97 E +2	7.46 E +2	7.80 E +2	9.51 E +2
35.0	35.7	1.96 E +2	1.79 E +2	1.86 E +2	2.17 E +2	2.38 E +2	3.26 E +2	3.47 E +2	3.67 E +2	4.50 E +2
40.0	40.8	1.15 E +2	9.61 E +1	9.40 E +1	9.74 E +1	9.98 E +1	1.14 E +2	1.34 E +2	1.59 E +2	2.05 E +2
45.0	45.9	5.00 E +1	3.84 E +1	3.46 E +1	3.27 E +1	3.12 E +1	5.84 E +1	7.73 E +1	9.22 E +1	1.21 E +2
50.0	51.0	2.32 E +1	1.89 E +1	1.68 E +1	1.62 E +1	2.02 E +1	6.05 E +1	6.76 E +1	6.71 E +1	8.13 E +1
55.0	56.1	1.57 E +1	1.35 E +1	1.35 E +1	1.43 E +1	2.00 E +1	5.23 E +1	5.00 E +1	4.02 E +1	4.90 E +1
60.0	61.1	1.03 E +1	9.01 E +0	1.01 E +1	1.12 E +1	1.30 E +1	2.70 E +1	2.43 E +1	1.84 E +1	2.38 E +1
65.0	66.2	6.39 E +0	5.69 E +0	6.85 E +0	8.08 E +0	9.54 E +0	9.24 E +0	8.98 E +0	1.01 E +1	1.37 E +1
70.0	71.2	5.39 E +0	4.92 E +0	5.29 E +0	6.15 E +0	6.07 E +0	4.42 E +0	6.08 E +0	9.34 E +0	1.23 E +1
75.0	76.2	5.31 E +0	4.85 E +0	4.34 E +0	4.54 E +0	3.82 E +0	6.12 E +0	7.24 E +0	8.37 E +0	1.08 E +1
80.0	81.3	4.43 E +0	3.61 E +0	2.84 E +0	2.60 E +0	2.13 E +0	7.16 E +0	7.37 E +0	5.86 E +0	7.62 E +0
85.0	86.3	2.56 E +0	1.94 E +0	1.35 E +0	1.14 E +0	1.29 E +0	5.85 E +0	5.12 E +0	3.32 E +0	4.22 E +0
90.0	91.3	1.03 E +0	8.06 E −1	6.72 E −1	7.88 E −1	1.29 E +0	3.53 E +0	2.75 E +0	1.89 E +0	2.42 E +0
95.0	96.3	5.15 E −1	6.57 E −1	7.71 E −1	1.15 E +0	1.58 E +0	1.69 E +0	1.38 E +0	1.39 E +0	1.88 E +0
100.0	101.3	7.94 E −1	9.55 E −1	1.08 E +0	1.44 E +0	1.56 E +0	8.77 E −1	1.01 E +0	1.27 E +0	1.85 E +0
105.0	106.2	1.20 E +0	1.16 E +0	1.12 E +0	1.30 E +0	1.15 E +0	8.96 E −1	1.14 E +0	1.16 E +0	1.68 E +0
110.0	111.2	1.28 E +0	1.00 E +0	8.38 E −1	8.30 E −1	6.25 E −1	1.16 E +0	1.25 E +0	9.62 E −1	1.32 E+0
115.0	116.2	9.78 E −1	6.76 E −1	4.66 E −1	3.97 E −1	2.93 E −1	1.28 E +0	1.14 E +0	7.04 E −1	9.07 E −1
120.0	121.1	5.53 E −1	3.70 E −1	2.11 E −1	1.85 E −1	2.20 E −1	1.10 E +0	8.48 E −1	4.72 E −1	6.20 E −1
125.0	126.1	2.38 E −1	2.04 E −1	1.36 E −1	1.87 E −1	3.00 E −1	7.38 E −1	5.33 E −1	3.18 E −1	4.65 E −1
130.0	131.0	1.46 E −1	1.98 E −1	1.95 E −1	2.91 E −1	3.84 E −1	4.27 E −1	3.09 E −1	2.57 E −1	4.21 E −1
135.0	135.9	2.31 E −1	2.84 E −1	2.87 E −1	3.74 E −1	3.99 E −1	2.87 E −1	2.66 E −1	2.56 E −1	4.28 E −1
140.0	140.8	3.67 E −1	3.38 E −1	3.30 E −1	3.77 E −1	3.39 E −1	3.17 E −1	3.32 E −1	2.80 E −1	4.16 E −1
145.0	145.7	4.61 E −1	3.59 E −1	3.10 E −1	3.06 E −1	2.39 E −1	4.14 E −1	3.93 E −1	2.73 E −1	3.76 E −1
150.0	150.6	4.48 E −1	3.03 E −1	2.48 E −1	2.18 E −1	1.54 E −1	4.67 E −1	4.36 E −1	2.44 E −1	3.20 E −1
155.0	155.6	3.69 E −1	2.56 E −1	1.96 E −1	1.68 E −1	1.32 E −1	4.62 E −1	4.07 E −1	1.89 E −1	2.62 E −1
160.0	160.4	2.53 E −1	1.90 E −1	1.65 E −1	1.81 E −1	1.66 E −1	4.02 E −1	3.28 E −1	1.46 E −1	2.23 E −1
165.0	165.3	1.63 E −1	1.63 E −1	1.61 E −1	2.13 E −1	2.31 E −1	3.26 E −1	2.46 E −1	1.28 E −1	2.08 E −1

TABLE II *(Continued)*

^{120}Sn c.m. angles used.

Lab angle (exact)	c.m. angle (app.)	^{112}Cd(d,d) $\Sigma_{abs}=2.0\%$ $\Sigma_{rel}=2.0\%$ $\sigma_{c.m.}$ (mb/sr)	^{115}In(d,d) $\Sigma_{abs}=2.0\%$ $\Sigma_{rel}=2.0\%$ $\sigma_{c.m.}$ (mb/sr)	^{112}Sn(d,d) $\Sigma_{abs}=2.0\%$ $\Sigma_{rel}=2.0\%$ $\sigma_{c.m.}$ (mb/sr)	^{120}Sn(d,d) $\Sigma_{abs}=4.0\%$ $\Sigma_{rel}=2.0\%$ $\sigma_{c.m.}$ (mb/sr)	^{124}Sn(d,d) $\Sigma_{abs}=4.0\%$ $\Sigma_{rel}=2.0\%$ $\sigma_{c.m.}$ (mb/sr)	^{208}Pb(d,d) $\Sigma_{abs}=2.0\%$ $\Sigma_{rel}=2.0\%$ $\sigma_{c.m.}$ (mb/sr)	^{209}Bi(d,d) $\Sigma_{abs}=2.0\%$ $\Sigma_{rel}=2.0\%$ $\sigma_{c.m.}$ (mb/sr)	^{232}Th(d,d) $\Sigma_{abs}=3.0\%$ $\Sigma_{rel}=2.0\%$ $\sigma_{c.m.}$ (mb/sr)	^{nat}Pt(d,d) $\Sigma_{abs}=1.5\%$ $\Sigma_{rel}=1.0\%$ c.m. angle	$\sigma_{c.m.}$ (mb/sr)
5.0	5.1	...	...	...	3.13 E +6	...	...	...	...	20.2	3.24 E +4
10.0	10.2	1.74 E +5	1.80 E +5	1.86 E +5	1.91 E +5	2.04 E +5	5.31 E +5	5.44 E +5	6.28 E +5	30.3	5.65 E +3
15.0	15.2	3.25 E +4	3.39 E +4	3.67 E +4	3.65 E +4	3.75 E +4	1.08 E +5	1.08 E +5	1.26 E +5	40.4	1.32 E +3
20.0	20.3	9.05 E +3	9.56 E +3	1.04 E +4	9.64 E +3	1.02 E +4	3.44 E +4	3.60 E +4	3.96 E +4	50.5	4.18 E +2
25.0	25.4	2.66 E +3	2.83 E +3	3.22 E +3	2.88 E +3	2.98 E +3	1.50 E +4	1.49 E +4	1.75 E +4	60.5	1.41 E +2
30.0	30.5	1.08 E +3	1.12 E +3	1.24 E +3	1.17 E +3	1.22 E +3	6.57 E +3	6.78 E +3	8.16 E +3	70.6	6.61 E +1
35.0	35.6	5.12 E +2	5.44 E +2	5.94 E +2	5.82 E +2	6.14 E +2	3.07 E +3	3.07 E +3	4.02 E +3		
40.0	40.6	2.50 E +2	2.75 E +2	3.00 E +2	2.96 E +2	3.11 E +2	1.57 E +3	1.59 E +3	2.11 E +3		
45.0	45.7	1.39 E +2	1.54 E +2	1.68 E +2	1.59 E +2	1.61 E +2	9.01 E +2	9.21 E +2	1.17 E +3		
50.0	50.7	8.78 E +1	9.12 E +1	9.90 E +1	8.82 E +1	8.57 E +1	5.04 E +2	5.19 E +2	6.60 E +2		
55.0	55.8	4.88 E +1	4.86 E +1	5.38 E +1	4.61 E +1	4.58 E +1	2.73 E +2	2.85 E +2	3.75 E +2		
60.0	60.8	2.51 E +1	2.63 E +1	2.83 E +1	2.77 E +1	3.12 E +1	1.61 E +2	1.67 E +2	2.28 E +2		
65.0	65.9	1.78 E +1	2.05 E +1	2.05 E +1	2.35 E +1	2.74 E +1	1.16 E +2	1.20 E +2	1.52 E +2		
70.0	70.9	1.59 E +1	1.86 E +1	1.84 E +1	1.99 E +1	2.08 E +1	8.67 E +1	8.85 E +1	1.03 E +2		
75.0	75.9	1.20 E +1	1.35 E +1	1.45 E +1	1.29 E +1	1.17 E +1	5.73 E +1	5.87 E +1	6.84 E +1		
80.0	81.0	7.13 E +0	7.60 E +0	8.57 E +0	6.42 E +0	5.60 E +0	3.44 E +1	3.52 E +1	4.45 E +1		
85.0	86.0	3.75 E +0	3.91 E +0	4.42 E +0	3.67 E +0	3.99 E +0	2.32 E +1	2.46 E +1	3.08 E +1		
90.0	91.0	2.62 E +0	3.06 E +0	3.06 E +0	3.71 E +0	4.65 E +0	1.98 E +1	2.08 E +1	2.32 E +1		
95.0	96.0	2.54 E +0	3.22 E +0	3.11 E +0	3.90 E +0	4.39 E +0	1.72 E +1	1.79 E +1	1.78 E +1		
100.0	101.0	2.39 E +0	3.00 E +0	3.05 E +0	3.20 E +0	3.16 E +0	1.34 E +1	1.40 E +1	1.33 E +1		
105.0	105.9	1.91 E +0	2.25 E +0	2.48 E +0	2.05 E +0	1.79 E +0	9.06 E +0	9.71 E +0	9.94 E +0		
110.0	110.9	1.29 E +0	1.43 E +0	1.65 E +0	1.17 E +0	1.06 E +0	6.55 E +0	6.91 E +0	7.47 E +0		
115.0	115.9	8.23 E −1	9.03 E −1	1.02 E +0	8.52 E −1	9.88 E −1	5.49 E +0	5.73 E +0	6.02 E +0		
120.0	120.8	6.11 E −1	7.44 E −1	7.81 E −1	8.86 E −1	1.12 E +0	5.23 E +0	5.39 E +0	4.88 E +0		
125.0	125.8	5.73 E −1	7.66 E −1	7.58 E −1	9.73 E −1	1.10 E +0	4.81 E +0	5.01 E +0	4.18 E +0		
130.0	130.7	5.70 E −1	7.99 E −1	7.94 E −1	9.14 E −1	9.35 E −1	4.08 E +0	4.28 E +0	3.56 E +0		
135.0	135.7	5.41 E −1	7.29 E −1	7.73 E −1	7.56 E −1	6.80 E −1	3.23 E +0	3.40 E +0	2.93 E +0		
140.0	140.6	4.69 E −1	5.97 E −1	6.67 E −1	5.47 E −1	5.02 E −1	2.68 E +0	2.81 E +0	2.47 E +0		
145.0	145.6	3.70 E −1	4.44 E −1	5.17 E −1	4.08 E −1	4.22 E −1	2.47 E +0	2.58 E +0			
150.0	150.5	2.84 E −1	3.34 E −1	3.90 E −1	3.29 E −1	4.11 E −1	2.41 E +0	2.52 E +0			
155.0	155.4	2.34 E −1	2.88 E −1	3.24 E −1	3.31 E −1	4.35 E −1	2.45 E +0	2.52 E +0			
160.0	160.3	2.28 E −1	3.04 E −1	3.32 E −1	3.57 E −1	4.45 E −1	2.36 E +0	2.36 E +0			
165.0	165.2	2.55 E −1	3.64 E −1	3.87 E −1	4.02 E −1	4.26 E −1	2.18 E +0	2.19 E +0			

F. Experimental errors

The duration of each run was chosen such that every elastic peak had $\gtrsim 10000$ counts, i.e., better than 1% statistics. Each data point was measured an average of 3 times. The relative discrepancies obtained from these overlaps were generally $\leq 1\%$, but always less than 2%. The angular resolution $\Delta\theta$ in the scattering plane ranged from ~0.3° for small angles, and 0.5° for medium angles (40–100°), to about 1° for back angles where the cross sections were lowest. No corrections for the finite size of $\Delta\theta$ were made.

With the tight slit configuration employed the beam divergence was $<\pm 0.15°$, and the zero degree shift or θ uncertainty from day to day was below 0.1°. This was verified by frequent measurements taken at ±10° which agreed to within $\lesssim \pm 5\%$, the difference predicted from a 0.1° shift in pure Rutherford scattering.

The standard foils of natural Pt were weighed and measured frequently with different balances, and their thicknesses have been determined as 5.85 mg/cm^2 ±1%. Using several of these foils the 17-MeV Pt(d, d) distribution at low angles has been determined to within 1.5% absolute accuracy (see Table II) from which the detector solid angles and efficiencies were obtained.

The probability of finding all elastically scattered deuterons under the elastic peak is smaller than 1.00 even in good detectors, as nuclear reaction of deuterons with silicon in the detectors are not completely negligible. King *et al.*[36] bombarded Si(Li) detectors directly with a 17-MeV deuteron beam and found that 99.37% of the incident flux was recorded as a single (full energy) deuteron peak. This effect of $\gtrsim 0.6\%$ would be augmented by poor collection after radiation damage or by slit scattering tails.

The agreement between thicknesses determined by weighing foils and target thicknesses determined from Rutherford scattering was within ~1% for ^{52}Cr, ^{56}Fe, and ^{nat}Pt and within ~4% for ^{232}Th.

The normalization discrepancies of $\gtrsim 3\%$ could be explained by target thickness variations. Total scale errors for each target are always below 5% (except for ^{48}Ca) and are listed individually in Tables II.

III. OPTICAL MODEL CALCULATIONS

The experimental data were fitted with optical potentials using the optical model codes HUNTER[37] and JIB.[38] We used a potential form which has been standard for deuteron scattering analysis, including a real potential part, a surface derivative part, a real spin orbit term of the Thomas form, and a Coulomb term:

$$V(r) = -Vf(r, r_0, a_0) + i\,4a_I W_D \frac{d}{dr} f(r, r_I, a_I) + V_{so}\left(\frac{\hbar}{m_\pi c}\right)^2 (\vec{\sigma}\cdot\vec{l})\frac{1}{r}\frac{d}{dr} f(r, r_{so}, a_{so}) + V_{Coul},$$

where the Woods-Saxon well f is given by

$$f(r, r_i, a_i) = \left[1 + \exp\left(\frac{r - r_i A^{1/3}}{a_i}\right)\right]^{-1};$$

A is the target mass number. The square of the pion Compton wavelength $(\hbar/m_\pi c)^2 = 2.00$ fm^2 is a conventional normalization factor. The Coulomb term is taken as the potential for a uniformly charged sphere of radius $R_c = 1.3A^{1/3}$.

The search codes can vary any specified combination of potential parameters such that χ^2, a goodness of fit quantity, is optimized. This quantity is defined as

$$\chi^2 = \frac{1}{N}\sum_{i=1}^{N}\left(\frac{\sigma_i^{th} - \sigma_i^{exp}}{\Delta\sigma_i^{exp}}\right)^2,$$

where σ_i^{th} and σ_i^{exp} are the theoretical and experimental cross sections at angle i, $\Delta\sigma_i^{exp}$ is the corresponding experimental error, and N is the number of points in the distribution.

Discrete ambiguities in the real well depth have always been present in the analysis of composite projectile scattering. In particular, comparable fits to (d, d) distributions have been generally obtained with the real well depth $V = nV_N$ where the nucleon depth $V_N \approx 50$ MeV and n is an integer. Elastic scattering data alone are generally not sufficient to resolve this ambiguity. However, the deuteron potential can be derived theoretically from folding the proton and neutron potentials,[23–30] giving a depth of $V_d \sim 100$ MeV, or more uniquely a volume integral per particle of $J_R/A_T A_p \approx 400$ MeV fm^3. It has also been found that more acceptable distorted-wave Born-approximation (DWBA) fits are obtained to deuteron stripping data with this "deep" deuteron potential.[39–41] Thus we have confined our searches to the family which most nearly yields a volume integral per particle of $J_R/2A_T \approx 400$ MeV fm^3.

Continuous ambiguities in optical parameters are manifested particularly in our work by the $V(r_0)$ correlation. Almost equally good fits could be obtained with r_0 in the range of 1.0 to 1.2 fm *provided* the real well depth was compensated for by roughly $Vr^{1.4} = \text{const}$. Since r_0 is not well defined at these energies, we hold the real radius parameter fixed for fits in which parameter systematics are being sought.

It was found that constraining r_0 to a fixed value for all targets yielded a rather well defined av-

erage a_0 for the real diffuseness a. Hence, it was decided to perform the analysis using fixed real geometry sets (r_0, a_0) of (1.0, 0.90) and (1.1, 0.82). In addition the set (1.2, 0.75) was also chosen to provide "well-matched" parameters for our own DWBA analyses.[42]

Our choice of a spin-orbit potential is somewhat tentative due to the lack of 17-MeV polarization data. Recent surveys[43-45] indicate that even polarization data do not determine the spin-orbit terms unambiguously. Recently, Knutson and Haeberli[31] successfully used a deuteron spin-dependent potential, derived from the folding of neutron and proton scattering, to simultaneously fit cross section data and vector and tensor analyzing powers on ^{90}Zr. We have been using the effective (spin 1) Thomas form of this folded potential in our analysis; i.e., $V_{so} = 5.63$ MeV, $r_{so} = 0.92$ fm, $a_{so} = 1.0$ fm.

A number of searches were made with both spin $=\frac{1}{2}$[38] and spin $= 1$[37] codes. Very little difference was found in either the parameters or the χ^2 values between the two formalisms, except for the spin-orbit depth itself. We determined that $V_{so}(\text{spin} = \frac{1}{2}) \approx \frac{3}{4} V_{so}(\text{spin} = 1)$, in agreement with Fitz *et al.*[3] with only this difference: spin $=\frac{1}{2}$ calculations at 17 MeV will reproduce spin $= 1$ predictions for cross sections to within a couple of per cent, except for deep structure at back angles in low-A targets.

IV. RESULTS AND DISCUSSION

A. Comparison of data and theory

Data points and theoretical fits to 23 angular distributions are plotted in Fig. 5, and tabulated in Table II. Although in general the data were taken in 5° steps from $\theta_{lab} = 10$ to 165°, the ^{27}Al angular distribution was measured in 2.5° steps up to only $\theta_{lab} = 100°$. This limitation arose because the kinematic energy loss of the scattered deuterons at back angles is such that the detector set available was not suitable for separating elastically scattered deuterons from the proton "background." With ^{232}Th, the maximum scattering angle was 140°, roughly the highest angle to which our spectrograph can be rotated. The ^{48}Ca(d, d) experiment was performed previously at this laboratory by Orloff. The absolute scale uncertainty is much higher than that for other targets and believed to be 10%.

Tables III–V list the best fit optical model parameters for the three real geometry sets $(r_0, a_0) = (1.0, 0.90)$, (1.1, 0.82), (1.2, 0.75). Included are the first three moments of the real potential, the volume integral of the imaginary potential, the calculated reaction cross section, and the χ^2 value based on experimental errors listed in Tables I and II.

Comparison of relative χ^2's indicates that the best fits occur with a real radius between 1.0 and 1.1 fm, although the 17-MeV data for heavier targets seem much less sensitive to the choice of real geometry. With the exception of ^{48}Ca, the real potential depth is well correlated with the Coulomb parameter $Z/A^{1/3}$ for all three geometry sets, as shown in Fig. 6. (The finite size of the deuteron could be responsible for the slightly nonlinear correlation.)

As the geometry of the real potential was fixed any structure effects would show more strongly in the imaginary part of the scattering potential.

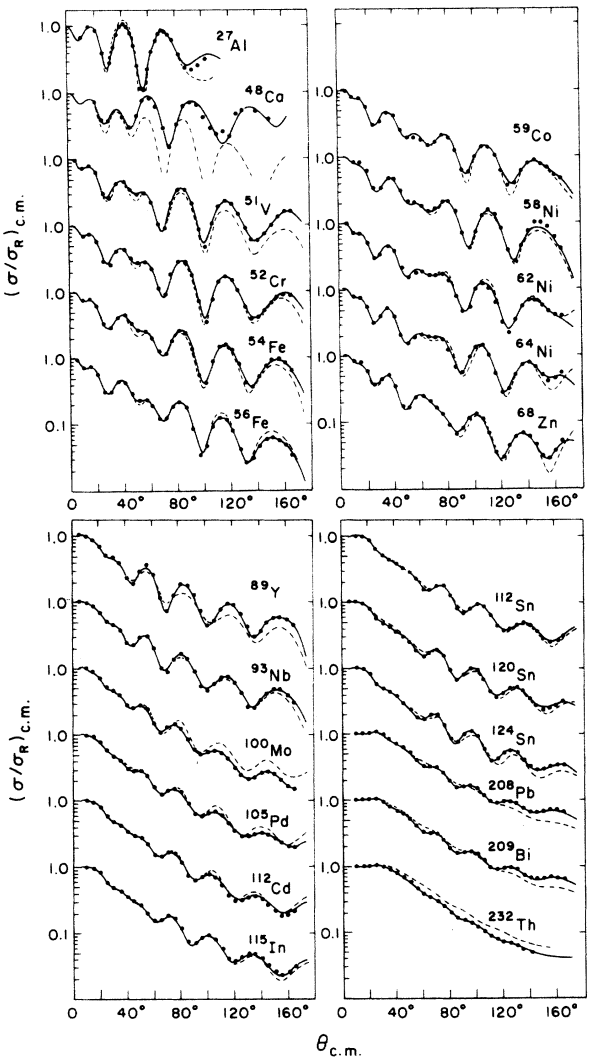

FIG. 5. 17-MeV (d, d) angular distributions. Solid lines represent the best fits listed in Table VI. The dashed lines represent the best global fit prescription given in the text. Note that the point size is larger than the experimental errors (except for ^{48}Ca).

It appears that the imaginary geometry parameters are noticeably affected by the fullness of the shells. For example, the average of the imaginary geometry parameters for fits with $r_0 = 1.0$ fm has the following values (see Table III):

$$\left.\begin{aligned} r_I &= 1.41 \pm 0.07 \text{ fm} \\ a_I &= 0.71 \pm 0.09 \text{ fm} \end{aligned}\right\} \text{ closed or semiclosed shell nuclei}$$

$$\left.\begin{aligned} r_I &= 1.33 \pm 0.04 \text{ fm} \\ a_I &= 0.78 \pm 0.09 \text{ fm} \end{aligned}\right\} \text{ both shells open .}$$

The imaginary strength W_D, however, is somewhat less correlated.

The best over-all nine-parameter fits are listed in Table VI. These were obtained by releasing the fixed spin-orbit and real geometry parameters used in the fits in Tables III–V. Generally, convergence to these nine-parameter best fits occurred uniquely from all three restricted best fit sets except for $A \geq 208$, where parameter ambiguities yield a range of equally good "best fits."

It is generally believed that the volume integral $J_R/2A_T$ for fits within a discrete parameter family is a fairly unique number.[46,47] We find here that it does vary less slowly than most other parameters, but still shows a continuous ambiguity related to the real parameter geometries. As can be seen from Tables III–V, J_R increases about linearly with the radius parameter r_0. For ^{68}Zn,

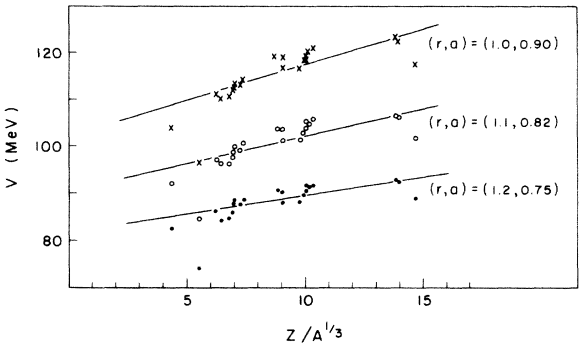

FIG. 6. Real well depth dependence on $Z/A^{1/3}$.

which shows a typical behavior, the dependence is approximately

$$J_R/2A_T \approx 150 + 200\, r_0 \text{ (fm)} \quad (\text{MeV fm}^3) .$$

For the radius parameter $r_0 = 1.10$ fm, which provides the best over-all fits, $J_R/2A_T$ decreases gradually from 410 MeV fm^3 for Al to 342 MeV fm^3 for ^{209}Bi. A similar, approximately 17% decrease from Al to Bi is also found for $r_0 = 1.0$. The decrease for $r_0 = 1.20$ is about 12% over the same mass range. The $J_R/2A_T$ numbers are fairly close to those obtained by Becchetti and Greenlees for proton scattering,[48] but as expected[29,30] a few percent smaller.

The smallest, but not negligible continous am-

TABLE III. Optical model parameters for best fits with real geometry $(r,a)_0 = (1.0, 0.90)$. Spin-orbit term fixed as in Ref. 31.

Target	V (MeV)	W_D (MeV)	r_I (fm)	a_I (fm)	σ_R (mb/sr)	χ^2	$J_R/2A_T$ (MeV fm^3)	$\langle r^2\rangle^{1/2}$ (fm)	$\langle r^4\rangle^{1/4}$ (fm)	$J_I/2A_T$ (MeV fm^3)
^{27}Al	104.0	9.43	1.39	0.77	1400	36.0	412.5	4.070	4.730	130.7
^{48}Ca	96.6	16.01	1.53	0.51	1480	2.5	325.3	4.371	5.005	135.8
^{51}V	110.9	14.85	1.44	0.63	1580	4.2	367.6	4.408	5.040	137.5
^{52}Cr	110.1	16.09	1.39	0.66	1580	5.8	363.2	4.420	5.051	145.5
^{54}Fe	111.7	16.57	1.39	0.65	1560	12.0	365.1	4.444	5.073	145.3
^{56}Fe	110.5	16.80	1.35	0.71	1630	4.6	358.1	4.468	5.096	151.7
^{59}Co	112.0	16.81	1.38	0.69	1650	5.3	358.5	4.503	5.128	150.3
^{58}Ni	112.9	15.57	1.39	0.68	1600	7.2	362.9	4.491	5.118	139.8
^{62}Ni	113.3	16.31	1.35	0.71	1670	2.2	358.6	4.537	5.160	141.8
^{64}Ni	113.2	15.42	1.38	0.70	1700	6.6	355.7	4.559	5.181	136.0
^{68}Zn	114.1	16.33	1.36	0.71	1700	4.2	353.8	4.602	5.221	139.2
^{89}Y	119.2	14.68	1.35	0.67	1650	8.7	349.9	4.811	5.418	105.0
^{93}Nb	118.8	14.78	1.32	0.72	1690	3.2	345.8	4.848	5.453	107.8
^{100}Mo	116.5	15.50	1.28	0.84	1900	0.4	334.6	4.911	5.514	123.1
^{105}Pd	116.3	15.38	1.30	0.82	1840	2.0	331.1	4.954	5.555	120.2
^{112}Cd	118.1	15.24	1.29	0.82	1830	1.1	332.5	5.013	5.611	114.6
^{115}In	119.3	15.04	1.31	0.77	1760	2.8	334.4	5.038	5.635	107.6
^{112}Sn	120.9	15.24	1.31	0.76	1700	2.8	340.4	5.013	5.611	108.6
^{120}Sn	120.2	13.93	1.33	0.78	1810	2.8	334.5	5.078	5.674	102.5
^{124}Sn	116.5	11.37	1.40	0.82	2000	2.2	328.0	5.110	5.704	96.3
^{208}Pb	123.1	7.82	1.51	0.81	1880	3.1	316.5	5.679	6.257	62.9
^{209}Bi	122.5	7.73	1.53	0.81	1900	2.2	314.8	5.685	6.263	63.7
^{232}Th	117.3	9.56	1.36	1.00	1900	0.6	297.7	5.818	6.393	75.7

TABLE IV. Optical model parameters for best fits with real geometry $(r,a)_0 = (1.1, 0.82)$. Spin-orbit term fixed as in Ref. 31.

Target	V (MeV)	W_D (MeV)	r_I (fm)	a_I (fm)	σ_R (mb/sr)	χ^2	$J_R/2A_T$ (MeV fm^3)	$\langle r^2\rangle^{1/2}$ (fm)	$\langle r^4\rangle^{1/4}$ (fm)	$J_I/2A_T$ (MeV fm^3)
^{27}Al	92.0	7.94	1.23	0.97	1480	36.0	413.2	3.977	4.557	119.5
^{48}Ca	84.3	16.04	1.52	0.51	1460	3.5	332.7	4.345	4.900	134.4
^{51}V	97.1	13.42	1.42	0.66	1570	4.1	378.7	4.390	4.943	127.3
^{52}Cr	95.9	14.89	1.38	0.68	1570	3.6	372.7	4.405	4.957	137.3
^{54}Fe	97.5	15.82	1.37	0.66	1530	3.6	376.2	4.434	4.985	137.3
^{56}Fe	96.3	16.12	1.33	0.72	1610	1.2	368.9	4.462	5.012	143.7
^{59}Co	98.7	16.94	1.35	0.68	1610	7.3	374.8	4.504	5.052	143.0
^{58}Ni	99.0	15.57	1.37	0.67	1560	2.6	377.1	4.491	5.039	133.8
^{62}Ni	99.9	16.57	1.32	0.70	1610	3.0	376.0	4.545	5.091	135.9
^{64}Ni	99.9	16.00	1.34	0.68	1630	8.4	374.0	4.572	5.117	129.2
^{68}Zn	100.5	17.42	1.32	0.68	1630	5.8	372.4	4.624	5.167	133.7
^{89}Y	103.7	15.47	1.32	0.66	1600	5.0	368.6	4.874	5.408	104.3
^{93}Nb	103.4	15.67	1.30	0.70	1640	2.6	365.3	4.918	5.451	107.6
^{100}Mo	101.2	16.06	1.25	0.84	1850	0.5	353.9	4.993	5.524	122.0
^{105}Pd	101.2	16.30	1.27	0.81	1780	2.2	351.6	5.045	5.574	120.3
^{112}Cd	102.7	16.08	1.26	0.82	1790	1.7	353.9	5.115	5.642	115.7
^{115}In	103.7	15.72	1.29	0.77	1740	3.4	356.1	5.144	5.671	109.3
^{112}Sn	105.4	16.54	1.28	0.75	1650	3.4	363.2	5.115	5.642	111.1
^{120}Sn	104.6	14.66	1.30	0.77	1760	2.6	357.3	5.192	5.717	101.8
^{124}Sn	105.1	13.85	1.31	0.77	1800	2.4	357.6	5.229	5.754	96.5
^{208}Pb	106.2	7.56	1.51	0.82	1890	2.5	342.3	5.897	6.415	61.6
^{209}Bi	106.0	7.66	1.52	0.82	1900	1.7	341.5	5.904	6.422	63.1
^{232}Th	101.6	10.81	1.33	1.02	1900	0.8	324.4	6.058	6.575	83.9

TABLE V. Optical model parameters for best fits with real geometry $(r,a)_0 = (1.2, 0.75)$. Spin-orbit term fixed as in Ref. 31.

Target	V (MeV)	W_D (MeV)	r_I (fm)	a_I (fm)	σ_R (mb/sr)	χ^2	$J_R/2A_T$ (MeV fm^3)	$\langle r^2\rangle^{1/2}$ (fm)	$\langle r^4\rangle^{1/4}$ (fm)	$J_I/2A_T$ (MeV fm^3)
^{27}Al	82.5	7.81	0.84	1.32	1630	34.0	426.6	3.943	4.454	111.1
^{48}Ca	74.1	17.25	1.49	0.52	1450	5.5	346.5	4.380	4.871	140.5
^{51}V	86.1	12.30	1.34	0.72	1545	9.7	399.0	4.433	4.922	114.3
^{52}Cr	84.0	14.68	1.35	0.69	1550	13.0	388.2	4.451	4.939	132.0
^{54}Fe	85.8	16.60	1.35	0.64	1490	5.6	394.3	4.485	4.973	135.4
^{56}Fe	84.5	16.67	1.31	0.71	1580	4.6	386.4	4.519	5.005	142.2
^{59}Co	87.6	18.10	1.33	0.65	1550	13.0	397.7	4.568	5.053	141.3
^{58}Ni	87.6	16.70	1.34	0.64	1500	3.0	398.6	4.552	5.037	130.8
^{62}Ni	88.5	18.10	1.29	0.66	1550	5.1	399.1	4.616	5.100	133.2
^{64}Ni	88.5	17.90	1.31	0.64	1560	14.4	397.5	4.647	5.130	129.6
^{68}Zn	88.4	18.85	1.30	0.65	1590	8.9	394.0	4.708	5.190	133.8
^{89}Y	90.5	17.10	1.31	0.63	1570	7.9	390.9	4.999	5.476	108.0
^{93}Nb	90.2	17.27	1.28	0.67	1610	4.8	387.8	5.050	5.526	109.8
^{100}Mo	87.9	17.06	1.22	0.84	1830	1.8	375.0	5.137	5.612	123.8
^{105}Pd	88.1	17.60	1.24	0.80	1750	4.6	374.1	5.196	5.671	122.4
^{112}Cd	89.5	17.20	1.23	0.82	1760	3.4	377.7	5.277	5.751	118.3
^{115}In	90.5	16.90	1.26	0.76	1710	4.5	380.9	5.311	5.784	110.7
^{112}Sn	91.6	17.20	1.27	0.75	1650	3.9	386.5	5.277	5.751	113.8
^{120}Sn	91.4	16.70	1.26	0.75	1700	2.9	383.2	5.366	5.839	106.2
^{124}Sn	91.7	16.30	1.28	0.74	1740	2.3	383.3	5.409	5.882	104.0
^{208}Pb	92.7	7.76	1.51	0.82	1890	4.2	372.3	6.173	6.648	63.2
^{209}Bi	92.4	7.77	1.52	0.82	1910	3.0	371.0	6.181	6.656	64.0
^{232}Th	88.7	13.00	1.27	1.04	1880	0.7	353.8	6.356	6.833	94.4

biguity is shown by the real root mean square radii which remained stable within 2–4% for ±20% changes in r_0 and corresponding ∓20% changes in V_0.

B. "Global" fits for 17-MeV data

The generally regular, smooth behavior of the parameters and the remaining ambiguities just mentioned suggest the usefulness and likely success for a global fit of the 17-MeV scattering data. We have attempted such fits with Perey's code GENOA,[49] omitting initially any energy or isospin-dependent functions for the parameters, but permitting r_0 and a_0 as well as r_I and a_I to find new best average values for the entire set (23 angular distributions) of simultaneously fitted data. With the exception of ^{48}Ca all angular distributions were fitted acceptably well with the parameters and relations:

$r_0 = 1.1$ fm $\quad a_0 = 0.82$ fm $\quad V = (85.6 + 1.79Z/A^{1/3})$ MeV

$r_I = (1.01 + 1.26A^{-1/3})$ fm $\quad a_I = (0.38 + 0.083A^{1/3})$ fm $\quad W_D = 15.9$ MeV

$r_{so} = 0.98$ fm $\quad a_{so} = 1.00$ fm $\quad V_{so} = 5.63$ MeV.

The quantities r_{so}, a_{so}, and V_{so} are not varied. In obtaining this prescription, the individual data sets were weighed by means of the χ^2's of their individual four-parameter best fits.

The predictions with this set of parameters, represented by dashed lines in Fig. 5, have an average χ^2 of ~20 (excepting ^{48}Ca) and should serve as a very useful means to approximate scattered waves or phase shifts for other non-deformed targets for $50 < A < 232$ at 17-MeV deuteron energy. The geometrical and real well depth parameters fall well within the range expected from folding calculations, whereas the $\vec{\sigma}\cdot\vec{l}$ potential is directly the result of such a prediction, in agreement with experiment,[31] but not uniquely determined by it.

Our preliminary parameter prescription above may have to be refined as other and higher energy data are included in the global analysis. However, our searches to date indicate that no drastic change in geometrical parameters (which are kept energy independent) is needed so that further (especially E-dependent) parameters should leave the global prescription for 17-MeV parameters relatively

TABLE VI. Optical model parameters for best nine-parameter fits, obtained by releasing constrained parameters of Tables III–V.

Target	V (MeV)	r_0 (fm)	a_0 (fm)	W_D (MeV)	r_I (fm)	a_I (fm)	V_{so} (MeV)	r_{so} (fm)	a_{so} (fm)	σ_R (mb/sr)	χ^2	$J_R/2A_T$ (MeV fm^3)	$\langle r^2\rangle^{1/2}$ (fm)	$\langle r^4\rangle^{1/4}$ (fm)	$J_I/2A_T$ (MeV fm^3)
^{27}Al	112.5	0.96	0.82	10.60	1.32	0.79	14.00	0.82	1.17	1340	0.8	376.1	3.775	4.372	138.2
^{48}Ca	112.6	0.91	0.88	14.00	1.52	0.53	7.23	0.75	0.98	1460	1.9	302.4	4.153	4.783	122.1
^{51}V	94.6	1.13	0.74	11.60	1.34	0.75	7.81	0.76	1.73	1550	0.9	373.9	4.255	4.741	113.8
^{52}Cr	92.6	1.14	0.75	13.30	1.31	0.74	6.59	1.03	1.46	1540	1.6	375.5	4.317	4.810	122.3
^{54}Fe	90.6	1.17	0.71	12.00	1.30	0.78	7.13	0.64	0.71	1540	0.9	381.2	4.324	4.784	113.9
^{56}Fe	94.8	1.12	0.79	15.30	1.32	0.74	6.60	0.90	1.16	1610	1.0	372.6	4.431	4.955	138.7
^{59}Co	104.6	1.05	0.86	16.10	1.36	0.68	7.47	0.93	1.63	1620	3.3	364.5	4.499	5.084	137.8
^{58}Ni	96.5	1.12	0.80	15.20	1.34	0.69	6.67	0.87	1.62	1550	2.0	379.4	4.485	5.016	129.4
^{62}Ni	114.5	0.99	0.90	15.00	1.35	0.72	8.88	0.62	1.72	1660	1.5	354.1	4.516	5.141	132.5
^{64}Ni	99.8	1.10	0.82	14.10	1.36	0.73	7.07	0.94	0.42	1700	0.9	373.6	4.572	5.117	126.7
^{68}Zn	107.2	1.06	0.84	14.10	1.35	0.75	7.20	0.92	0.28	1700	0.9	367.0	4.580	5.143	125.9
^{89}Y	98.2	1.14	0.81	13.30	1.35	0.69	7.28	1.05	0.51	1670	1.7	380.9	4.961	5.484	98.2
^{93}Nb	99.0	1.12	0.84	16.70	1.31	0.64	5.63	1.42	1.20	1600	0.8	370.1	5.020	5.566	105.6
^{100}Mo	110.0	1.04	0.86	15.50	1.27	0.85	5.64	0.94	1.00	1880	0.3	340.4	4.919	5.486	122.9
^{105}Pd	104.1	1.07	0.88	15.40	1.32	0.80	6.45	1.06	0.64	1840	1.3	347.2	5.098	5.675	120.6
^{112}Cd	109.6	1.04	0.89	15.30	1.31	0.80	6.15	1.00	0.76	1840	0.5	338.6	5.101	5.687	115.3
^{115}In	108.2	1.06	0.91	13.90	1.36	0.75	7.24	0.96	0.81	1830	0.6	352.9	5.233	5.831	103.9
^{112}Sn	105.5	1.08	0.88	15.20	1.34	0.73	6.56	0.96	0.64	1740	0.6	356.9	5.192	5.766	108.2
^{120}Sn	105.7	1.07	0.90	12.20	1.39	0.78	8.47	1.16	0.29	1910	0.2	349.1	5.282	5.870	97.7
^{124}Sn	102.2	1.11	0.87	12.20	1.38	0.75	7.99	0.89	0.96	1890	0.3	364.1	5.370	5.931	91.3
^{208}Pb	108.3	1.09	0.93	8.69	1.45	0.71	10.59	0.67	1.85	1660	1.1	353.9	6.081	6.673	56.3
^{209}Bi	112.3	1.06	0.96	8.71	1.46	0.73	9.59	0.73	1.78	1700	0.6	344.5	6.039	6.656	58.7
^{232}Th	104.0	1.08	0.95	10.20	1.37	0.86	13.47	1.08	0.44	1730	0.1	329.9	6.236	6.841	69.7

unchanged.

Difficulty in fitting ^{232}Th would be expected since this nucleus is deformed, and low-lying states are strongly excited. Nevertheless, the global prediction at 17 MeV is reasonably close to the data.

The disagreement for ^{48}Ca is more drastic. The best fit parameters (Table VI) for this target show $r_0 = 0.91$, $a = 0.88$, and $J_R/2A_T = 302.4$ MeV fm^3, a significant deviation from all other best fit parameters. Although the ^{48}Ca data have the largest systematic error, we do not believe that experimental errors are responsible for this singular behavior. Scale adjustments of ±10% brought no improvements in the fits. Furthermore, other studies of elastic scattering of other projectiles from Ca isotopes also have shown unexpected behavior.[48]

Finally, it should be noted that at 17 MeV we seem to find a T or an $A^{1/3}$ dependence in the imaginary volume integral. In Table VI, for instance, $J_I/2A_T$ falls more or less linearly to half its value for ^{27}Al with $A^{1/3}$ or $N-Z$. The $(N-Z)$ dependence shows less scatter, but as the deuteron has $T=0$ a $(N-Z)$ or T dependence must have subtle reasons if it is not spurious. It is hoped that the simultaneous consideration of higher energy data now in progress may permit more definite statements.

ACKNOWLEDGMENTS

The authors appreciate the cooperation and assistance given by R. Gibson and R. DelVecchio. We are especially grateful to F. G. Perey for making the code GENOA available to us and for sponsoring a number of test runs at Oak Ridge National Laboratory. Thanks are also due to R. M. Drisko for a number of very helpful discussions.

---

*Work supported by the National Science Foundation.

[1]G. Igo, W. Lorenz, and U. Schmidt-Rohr, Phys. Rev. 124, 832 (1961).
[2]T. Becker, U. Schmidt-Rohr, and E. Tielsch, Phys. Lett. 5, 331 (1963).
[3]W. Fitz, J. Heger, R. Santo, and S. Wenneis, Nucl. Phys. A143, 113 (1970).
[4]M. Takeda, J. Phys. Soc. Jap. 15, 557 (1960).
[5]P. R. Christensen, A. Berinde, I. Neamu, and N. Scintei, Nucl. Phys. A129, 337 (1969).
[6]N. Cindro and N. S. Wall, Phys. Rev. 119, 1340 (1960).
[7]A. N. Vereshehagin, O. F. Nemets, L. S. Sokolov, I. P. Chernov, and A. A. Yatis, Izv. Akad. Nauk. SSSR, Ser. Fiz. 32 (12), 1956 (1968) [transl.: Bull. Acad. Sci. USSR, Phys. Ser. 32 (12), 1800 (1968)].
[8]S. A. Hjorth, E. K. Lin, and A. Johnson, Nucl. Phys. A116, 1 (1968).
[9]R. K. Jolly, E. K. Lin, and B. L. Cohen, Phys. Rev. 130, 2391 (1963).
[10]J. L. Yntema, Phys. Rev. 113, 261 (1959).
[11]H. R. E. Tjin a Djie, F. Udo, and L. A. Ch. Koerts, Nucl. Phys. 53, 625 (1964); 74, 417 (1965).
[12]J. Testoni, J. Rosenblatt, and S. Mayo, Nucl. Phys. 74, 481 (1965).
[13]E. Newman, L. C. Becker, and B. M. Preedom, Nucl. Phys. A100, 225 (1967).
[14]F. Hinterberger, G. Mairle, U. Schmidt-Rohr, and G. J. Wagner, Nucl. Phys. A111, 265 (1968).
[15]P. E. Hodgson, *The Optical Model of Elastic Scattering* (Clarendon, Oxford, England, 1963).
[16]C. M. Perey and F. G. Perey, Phys. Rev. 132, 755 (1963).
[17]C. M. Perey and F. G. Perey, Phys. Rev. 134, B353 (1964).
[18]C. M. Perey and F. G. Perey, Phys. Rev. 152, 923 (1966).
[19]E. C. Halbert, Nucl. Phys. 50, 353 (1964).
[20]G. R. Satchler, Nucl. Phys. 85, 273 (1966).
[21]P. Schwandt and W. Haeberli, Nucl. Phys. A132, 401 (1969).
[22]J. K. Dickens and F. G. Perey, Phys. Rev. 138, B1083 (1965).
[23]S. Watanabe, Nucl. Phys. 8, 484 (1958).
[24]J. R. Rook, Nucl. Phys. 61, 219 (1965).
[25]A. Y. Abul-Magd and M. El-Nadi, Prog. Theor. Phys. 35, 798 (1966).
[26]E. Coffou and L. J. B. Goldfarb, Nucl. Phys. A94, 241 (1967).
[27]F. G. Perey and G. R. Satchler, Nucl. Phys. A97, 515 (1967).
[28]M. El-Nadi and O. Zohni, Z. Phys. 206, 18 (1967).
[29]P. D. Kunz, Phys. Lett. 35B, 16 (1971).
[30]R. C. Johnson and P. J. R. Soper, Phys. Rev. C 1, 976 (1970); Nucl. Phys. A182, 619 (1972).
[31]L. D. Knutson and W. Haeberli, Phys. Rev. Lett. 30, 986 (1973).
[32]J. Childs, W. W. Daehnick, and M. Spisak, Bull. Am. Phys. Soc. 17, 535 (1972).
[33]J. Childs, W. W. Daehnick, and M. Spisak, Bull. Am. Phys. Soc. 18, 604 (1973).
[34]G. Lindstroem, Nucl. Instrum. Methods 56, 309 (1967).
[35]J. J. Kolata, R. F. Gibson, and J. Holden, Univ. of Pittsburgh, unpublished.
[36]T. R. King, J. J. Kraushaar, R. A. Ristinen, R. Smythe, and D. M. Stupin, Nucl. Instrum. Methods 88, 17 (1970).
[37]R. M. Drisko, unpublished.
[38]F. G. Perey, unpublished.
[39]P. T. Andrews, R. W. Clifft, L. L. Green, and J. F. Sharpey-Schafer, Nucl. Phys. 56, 465 (1964).
[40]L. L. Lee, Jr., J. P. Schiffer, B. Zeidman, G. R. Satchler, R. M. Drisko, and R. H. Bassel, Phys. Rev. 136, B971 (1964).
[41]J. L. Alty, L. L. Green, G. D. Jones, and J. F. Sharpey-Schafer, Nucl. Phys. A100, 191 (1967).
[42]R. M. DelVecchio and W. W. Daehnick, Phys. Rev. C 6,

2095 (1972).
[43]P. Schwandt and W. Haeberli, Nucl. Phys. A110, 585 (1968).
[44]J. A. R. Griffith, M. Irshad, O. Karban, and S. Roman, Nucl. Phys. A146, 193 (1970).
[45]G. Heil, G. Klier, and H. Wilsch, Nucl. Phys. A191, 489 (1972).
[46]G. W. Greenlees, G. J. Pyle, and Y. C. Tang, Phys. Rev. 171, 1115 (1968).
[47]M. E. Cage, A. J. Cole, and G. J. Pyle, Nucl. Phys. A201, 418 (1973).
[48]F. D. Becchetti and G. W. Greenlees, Phys. Rev. 182, 1190 (1969).
[49]F. G. Perey, unpublished.